INL/CON-12-24399
PREPRINT

Improved Neutronics Treatment of Burnable Poisons for the Prismatic HTR

HTR 2012

Y. Wang
A. A. Bingham
J. Ortensi
C. J. Permann

October 2012

The INL is a
U.S. Department of Energy
National Laboratory
operated by
Battelle Energy Alliance

Proceedings of the HTR 2012
Tokyo, Japan, October 28 – November 1, 2012
Paper HTR2012-5-016

Improved Neutronics Treatment of Burnable Poisons for the Prismatic HTR

Y. Wang, A. A. Bingham, J. Ortensi, C. J. Permann
Idaho National Laboratory
2525 North Fremont Avenue, Idaho Falls, ID, 83415, USA
phone: +1-208-526-0054,Yaqi.Wang@inl.gov

Abstract – *In prismatic block High Temperature Reactors (HTR), highly absorbing material such a burnable poison (BP) cause local flux depressions and large gradients in the flux across the blocks which can be a challenge to capture accurately with traditional homogenization methods. The purpose of this paper is to quantify the error associated with spatial homogenization, spectral condensation and discretization and to highlight what is needed for improved neutronics treatments of burnable poisons for the prismatic HTR. A new triangular based mesh is designed to separate the BP regions from the fuel assembly. A set of packages including Serpent (Monte Carlo), Xuthos (1st order Sn), Pronghorn (diffusion), INSTANT (Pn) and RattleSnake (2nd order Sn) is used for this study. The results from the deterministic calculations show that the cross sections generated directly in Serpent are not sufficient to accurately reproduce the reference Monte Carlo solution in all cases. The BP treatment produces good results, but this is mainly due to error cancellation. However, the Super Cell (SC) approach yields cross sections that are consistent with cross sections prepared on an "exact" full core calculation. In addition, very good agreement exists between the various deterministic transport and diffusion codes in both eigenvalue and power distributions. Future research will focus on improving the cross sections and quantifying the error cancellation.*

I. INTRODUCTION

It is essential for the analysis of prismatic HTRs to accurately determine the effects of Burnable Poison (BP) pins. Local effects from BP pins are less pronounced in an HTR core than in a Light Water Reactors (LWR). However, with burnable poison pins located in the corner of a block surrounded by reflector blocks on both adjacent sides, the flux depression can be quite significant. Additionally, due to the long neutron migration lengths in HTRs, the area of influence of BPs is spread over neighboring blocks. Error in calculation of the absorption reaction rates of these regions can have a significant impact on the local poison depletion and the isotopic distribution in the surrounding fuel as a function of time[1]. Consequently, these accumulative errors would affect power distribution and shutdown margin predictions through the cycle.

In a similar fashion to the method used by CEA in the analysis of the High Temperature Test Reactor (HTTR)[2], the Idaho National Laboratory (INL) has developed a triangular based mesh to isolate the BP regions with a new meshing routine available in Pronghorn[3], an application of the Multi-Physics Object Oriented Simulation Environment (MOOSE)[4].

A set of cross sections and a reference solution were prepared with the continuous energy Monte Carlo code Serpent[5, 6]. Unfortunately, the preparation of few group cross sections for HTR reactors from Monte Carlo calculations is not a well developed area. We aim to better understand this process and to improve our cross section preparation capability.

An investigation on how the BP affects the deterministic calculations is conducted with different neutron transport models. The codes used for the study are Pronghorn (diffusion), INSTANT (Pn) [7], Xuthos (Sn 1st order)[8] and RattleSnake (Sn 2nd order)[9]. Errors due to the spatial homogenization, group condensation, and discretization in space and angle are isolated through application of the different methods used by these codes.

II. MESH GENERATION

Right hexagonal prism graphite blocks characterize the prismatic HTR geometry. Fuel

holes and coolant channels run in parallel through the blocks. For neutronics calculations the in-core geometry is often homogenized on the whole block or in triangular prism regions. This homogenized geometry can be captured with a structured triangular mesh. The permanent reflector forms a cylinder around the core. To represent this geometry accurately an unstructured mesh is needed in the permanent reflector region. The capability to generate a combined structured and unstructured mesh for a prismatic HTR has been developed within the Pronghorn application. Burnable poison pins located in the corner of an assembly are modeled by local triangles in the corner as that illustrated in Fig. 1. Pronghorn utilizes libMesh[10] libraries to generate both 2D and 3D hexagonal based meshes in the core joined to an unstructured mesh in the permanent reflector for 1/3, 1/6, and 1/12 reflected core geometry. This capability was used to generate an Exodus [11] format mesh for Pronghorn, RattleSnake, and INSTANT calculations and a Planar Straight Line Graph (PSLG) mesh file for Xuthos. The unrefined mesh presented in Fig. 1 is the base mesh for deterministic calculations. The mesh contains total 19 regions of interest (6 BP regions, 7 fuel assemblies, 3 graphite blocks surrounding the BP assembly, and central, replaceable and permanent reflector).The radius of the outer reflector is 297.5 cm.

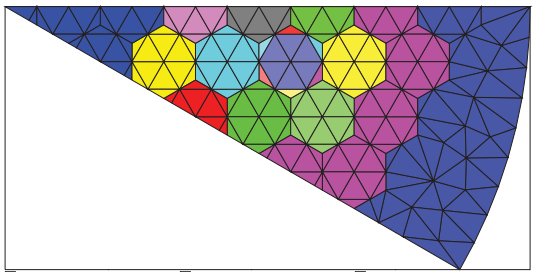

Fig. 1: The mesh with material mapping.

III. REFERENCE SOLUTION AND CROSS SECTION PREPARATION

The Serpent code, version 1.1.16, was used in both the generation of the reference solution and the preparation of cross sections. The nuclear data is from the ENDF/B-VII.r0. Serpent is a Monte Carlo (MC) continuous-energy neutron transport code developed at the VTT Technical Research Centre in Finland. Serpent was principally developed for pin and lattice burnup and cross section preparation.

Employing a MC code to prepare cross section removes the multigroup and self-shielding approximations commonly used in deterministic lattice physics codes. In addition, this approach significantly reduces the potential for human error. Therefore, the main sources of error arise from the relative error of the tallies used in the cross section preparation.

III.A. Geometric Models

The two geometric models used to generate cross sections in this study are the full core and Super Cell (SC).

The Serpent full core geometric model comprises the 2-D prismatic HTR shown in Fig. 2. The full core is modeled because Serpent 1.1.16 does not support a $1/12^{th}$ reactor geometry. The Serpent model utilizes homogenized regions to minimize the sources of error for this analysis. The various regions modeled include a central reflector, active core, replaceable reflector and permanent reflector. The active core region is primarily composed of once-burned fuel with the exception of one fresh fuel block, which contains the BPs. This block is modeled with six triangular regions defined at the corners, which match the mesh used in the deterministic codes. The burnable poison pins are the only regions within the fuel block that are explicitly represented in this model. Future calculations will include full compact representation throughout the core.

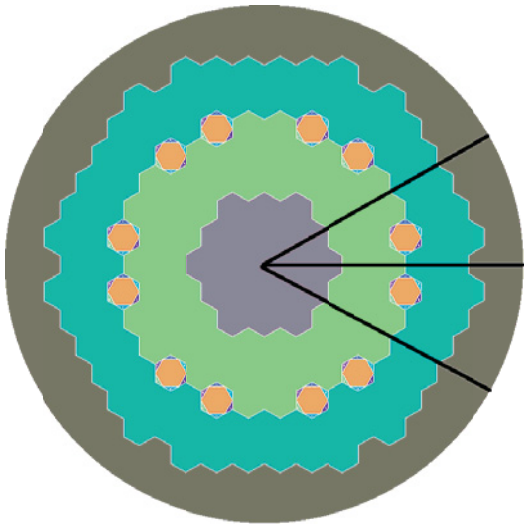

Fig. 2: Serpent full core geometric model.

The use of super cells has been shown to be an effective way to capture the effects from reflectors in the cross sections[12, 13]. These larger domains drastically improve the neutron spectrum used in the preparation of the cross sections for thin, annular

cores. Furthermore, it appears to be one of the limited mechanisms to prepare accurate cross sections for regions with BPs. The Serpent SC geometric model is shown in Fig. 3 and consists of a hexagonal region with 124.7 across-the-flats distance. This SC is representative of the $1/12^{th}$ core region being studied for cross section preparation. The center block of the super cell is the Region of Interest (ROI) for this study. The SC includes a once-burned fuel region to the left of the ROI and a reflector region to the right.

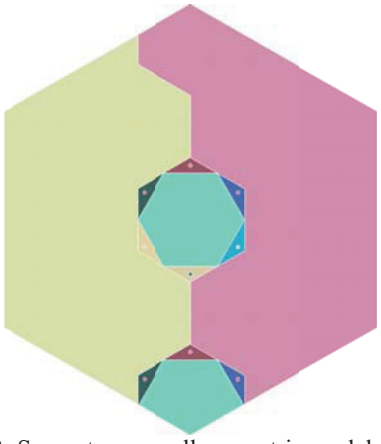

Fig.3: Serpent super cell geometric model with the Region of Interest in the center.

Four variations (cases) of the composition of the BP and triangular fill region are included in the study to better understand the separate effects of the various materials. The four configurations of the regions are:

1. graphite in the pin and fill materials
2. BP in pin and graphite in fill material
3. graphite in the pin and fresh fuel in fill material
4. BP in the pin and fresh fuel in fill material

III.B. Reference Solution

The Monte Carlo reference solution was obtained from Serpent with the full core model. The tallies included in the Serpent model are: 1) fission energy in the power generating regions, 2) integral and energy dependent neutron capture rate in the BP triangular regions, and 3) energy dependent flux in the ROI adjacent blocks. For the initial analysis we will focus on the eigenvalue and power distribution in the core.

A deterministic reference solution is also computed with the Xuthos code in order to assess the accuracy of the various codes given a set of cross sections from the full core model.

III.C. Cross Section Preparation

Two distinct cross section sets were prepared. The first set is generated from the full core calculation and is used to compute the Xuthos deterministic reference. The second set includes the same cross sections as the reference set for the exception of the ROI, which is generated via the SC.

Spatially the cross sections are homogenized in 11 distinct spectral regions: inner reflector, burned fuel, 6 BPs, central fresh fuel, replaceable reflector, and permanent reflector. The homogenization of the spent fuel blocks introduces a spatial discrepancy between the Monte Carlo and the deterministic calculations. However, since the cross-sections are fixed for the various cases this discrepancy should not significantly affect the results or conclusions of this study for comparisons among the deterministic results.

The diffusion coefficient is a parameter that is approximated and it has no real analog in continuous energy transport. Serpent employs two definitions of the diffusion coefficient[4] from the:

1) P_1 approximation

$$D^g = \frac{1}{3\left(\Sigma_t^g - \bar{\mu}_0^g \Sigma_s^g\right)} \quad (1)$$

2) Approximation based on the ratio of analog diffusion area to removal cross section

$$D^g = \frac{\overline{r_g^2}}{6\left(\Sigma_t^g - \Sigma_s^{g\to g}\right)} \quad (2)$$

where

D^g =group g diffusion coefficient

Σ_t^g =group g total cross section

$\bar{\mu}_0^g$ = group g average scattering cosine

Σ_s^g =group g total scattering cross section

$\overline{r_g^2}$ =mean squared distance of neutron migration

$\Sigma_s^{g\to g}$ =within group g scattering cross section

The first method is based on localized effects, which might not be optimal for the faster groups in HTRs due to longer mean free paths. In addition, there is real difficulty in determining the average scattering cosine. Overall, we would expect the second approach to be better for HTRs.

In addition to the four compositional variations of the triangular regions, 3 different coarse group structures are used in the cross section preparation and shown in Table 1. The 25 group structure is

derived from the 26 group structure developed by Jülich[2] by merging the top two groups. The nine-group structure is the General Atomics validated structure. The two-group structure was used in the OECD/NEA PBMR-400 benchmark[14].

25 group	9 group	2 group
3.33E+06		
7.07E+05		
	1.83E+05	
1.16E+05		
1.86E+04		
3.48E+03		
1.59E+03		
	9.61E+02	
7.49E+02		
2.76E+02		
1.33E+02		
6.23E+01		
3.17E+01		
	1.76E+01	
1.35E+01		
8.30E+00		
5.11E+00		
	3.93E+00	
		3.05E+00
	2.38E+00	
2.33E+00		
1.29E+00		
	1.28E+00	
	8.25E-01	
6.25E-01		
3.53E-01		
2.10E-01		
	1.30E-01	
1.20E-01		
7.65E-02		
5.55E-02		
2.00E-02		
1.05E-02		
0	0	0

Table 1: Coarse energy group lower boundaries in eV

IV. DIFFERENT DETERMINISTIC NEUTRONIC PACKAGES

A broad set of packages cover diffusion, Pn, Sn and different finite element methods are used for this study in order for us to give the recommendations on resolving the BP effect. We only focus ourselves on the discretization error of different models. CPU time is not our concern for this small problem. All solvers are converged with negligibly small iterative errors. All transport solvers can solve the problem with arbitrarily anisotropic scattering although only isotropic scattering cross sections are generated in this study.

II.A. Xuthos

Xuthos is a transport solver solving the original multigroup transport equation

$$\vec{\Omega}\cdot\vec{\nabla}\Psi_g+\sigma_{t,g}(\vec{r})\Psi_g(\vec{r},\vec{\Omega})=\frac{1}{4\pi}\sum_{g'=1}^{G}\sigma_s^{g'\to g}(\vec{r})\Phi_{g'}(\vec{r})+\frac{1}{k_{eff}}\frac{\chi_g(\vec{r})}{4\pi}\sum_{g'=1}^{G}\nu\sigma_{f,g'}(\vec{r})\Phi_{g'}(\vec{r})$$
$$g=1,\cdots,G;\quad \vec{r}\in D,\ \vec{\Omega}\in 2\text{D unit sphere} \tag{3}$$

with the vacuum boundary condition

$$\Psi_g(\vec{r}_b,\vec{\Omega})=0,\ \forall\vec{r}\in\partial D^s,\ \vec{\Omega}\cdot\vec{n}<0 \tag{4}$$

and the reflecting boundary condition

$$\Psi_g(\vec{r}_b,\vec{\Omega})=\Psi_g(\vec{r}_b,\vec{\Omega}-2(\vec{\Omega}\cdot\vec{n})\vec{n}),\ \forall\vec{r}\in\partial D^r,\ \vec{\Omega}\cdot\vec{n}<0 \tag{5}$$

with Sn and a higher-order discontinuous finite element method on 2D unstructured triangular grids. Because the streaming term in Eq. (1) contains the first-order spatial derivative of the angular flux, Eq. (1) is also called as the first-order transport equation. Because all cross sections used in this study are isotropic, the scattering term in Eq. (1) is defined with the scalar flux

$$\Phi_g(\vec{r})=\int_{4\pi}\Psi_g(\vec{r},\vec{\Omega})d\Omega\cdot \tag{6}$$

All the notations in Eq. (3) are standard in the text. The unique feature of Xuthos is its capability of performing the calculations with the spatial Adaptive Mesh Refinement (AMR) on group-dependent meshes[15]. With AMR, the user can control the spatial discretization error to a desired tolerance within a given multigroup cross section and the angular quadrature. The angular discretization can be refined by increasing the number of polar angles and the number of azimuthal angles with the Gauss-Chebyshev production quadrature. To insure the reflecting directions with the 30-degree boundary are also in the quadrature, the number of azimuthal angles must be given as an integer multiple of 3. Xuthos is used to generate the reference deterministic solution for each given multigroup cross section set in this study. Differences between Xuthos results and the Serpent results are assumed due only to spatial homogenization and group condensation.

II.B. Pronghorn

The Pronghorn code was designed to model reactor physics coupled to thermal-fluid in a pebble bed reactor (PBR) high temperature gas cooled reactor (HTR) built as an application of the MOOSE

finite element framework. Its neutronics part solves the multigroup diffusion equation

$$\vec{\nabla}\cdot(D_g\vec{\nabla}\Phi_g)+\sigma_{r,g}(\vec{r})\Phi_g(\vec{r})=\sum_{g'\neq g}\sigma_s^{g'\to g}(\vec{r})\Phi_{g'}(\vec{r})+\frac{1}{k_{eff}}\chi_g(\vec{r})\sum_{g'=1}^{G}\nu\sigma_{f,g'}(\vec{r})\Phi_{g'}(\vec{r}) \quad (7)$$
$$g=1,\cdots,G$$

where

$$\sigma_{r,g}(\vec{r})=\sigma_{t,g}(\vec{r})-\sigma_s^{g\to g}(\vec{r}) \quad (8)$$

with the continuous FEM.

The boundary condition for the diffusion equation is

$$\frac{1}{4}\Phi_g+\frac{1}{2}D_g\vec{\nabla}\Phi_g\cdot\vec{n}\Big|_{\vec{r}\in\partial D^s}=0$$
$$D_g\vec{\nabla}\Phi_g\cdot\vec{n}\Big|_{\vec{r}\in\partial D^r}=0 \quad (9)$$

No transport corrections are applied on the vacuum boundary. MOOSE supports spatial polynomial order up to 3, however first order Lagrange polynomials were used for the scalar flux solutions.

II.C. INSTANT

INSTANT solves the transport equation Eq. (3) in the even-odd parity form with the Pn (spherical harmonics expansion) in angle and the hybrid finite element method in space (also known as Variational Nodal Method (VNM)[16]). Pn order up to 33 is supported by INSTANT. The detailed weak form can be found in Ref[7].The build-in unstructured mesh framework makes INSTANT able to solve problems on 2D Cartesian, hexagonal and triangular meshes and 3D Cartesian, extruded hexagonal and triangular meshes in parallel. The spatial discretization error is controlled by two polynomial orders p_{int} (the polynomial order of shape functions used to expand the even parity interior of elements) and p_{surf} (the polynomial order of shape functions used to expand the odd parity over sides of elements),which must satisfy the rank condition. In this study we always set

$$p_{\text{int}}=p_{\text{surf}}+2 \quad (10)$$

and used the same order for all the triangles.

II.D. RattleSnake

RattleSnake is a radiation Sn transport application built using the MOOSE finite element framework. RattleSnake is designed to be easily inserted into a system from pin-resolved fuel performance analysis to full-core safety analysis for tightly coupled multiphysics simulations. RattleSnake solves the multigroup Sn transport equation Eq. (1) in the formulation of Self-Adjoint Angular Flux (SAAF)[17] with a continuous finite element method. It solves both the transient and eigenvalue problems. Because RattleSnake is based on MOOSE, it can solve problems on 2D and 3D unstructured higher-order meshes in parallel. The same Gauss-Chebyshev angular quadrature as Xuthos is used by RattleSnake. Uniform polynomial order is used in this study.

V. RESULTS

V.A. Xuthos deterministic reference results

We determined the angular convergence with case 1 and 2 groups by varying the number of polar angles and the number of azimuthal angles per octant. The errors of k-effective are plotted in Fig 4. The reference k-effective is generated with a significant larger number of polar angles equal to 32 and a larger number of azimuthal angles equal to 48 per octant.

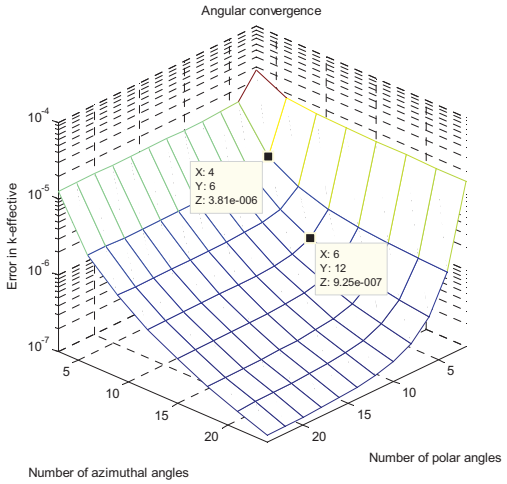

Fig 4: Angular convergence of k-effective with Xuthos.

We can see the k-effective converges to the reference one slightly faster with respect to the number of polar angles. The error is less than 1 pcm with 4 polar angles and 6 azimuthal angles. The

error is further reduced below 0.1 pcm with 6 polar angles and 12 azimuthal angles. To be more conservative, we later use 8 polar angles and 18 azimuthal angles to generate all reference results for all cases and all the number of energy groups.

The adapted group-dependent meshes are illustrated for case 4 with 9-group using the cross section set from the full core SERPENT calculation.

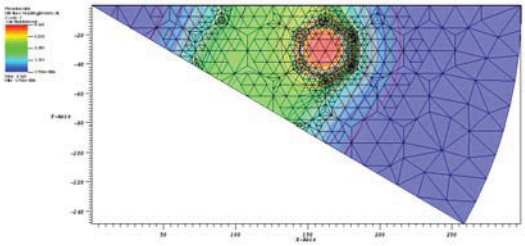

(b) Group 2

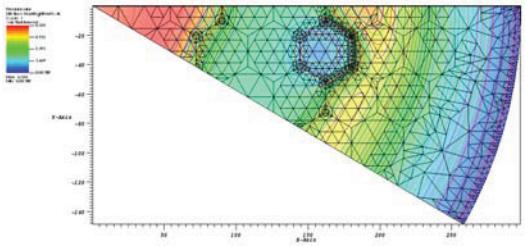

(h) Group 8

Fig. 5: 9-group adapted meshes.

The resulting meshes for the fast groups 1 to 5 have the similar elements. Likewise, the meshes for the epithermal groups 6 and 7and the thermal meshes of group 8 and 9have similar characteristics to each other. We only give a mesh of a representative fast group (group 2) and a mesh of a representing thermal group (group 8). The adapted meshes tend to be refined at the places where the solutions vary most rapidly. The adapted meshes can give us an idea on how the material discontinuity affects the solution.

The k-effective comparison with the FC cross section set is listed in Table 2. The results show that, with the exception of case 2, the eigenvalue estimation improves with the refinement of the group structure. In case two, the addition of extra moderator around the BP pin yields and under-prediction of the eigenvalue. Without the results from cases 1-3 one could conclude that the analysis approach works very well for main case of interest, case 4. Case 3 indicates that the solution in case 4 is improved due to error cancellation when the BP pins are introduced.

Table 2: Differences in k-effective (pcm) between Xuthos and Serpent with FC cross section set

		Case 1	Case 2	Case 3	Case 4
Xuthos	2 group	1328.2	394.7	1907.3	931.7
	9 group	529.1	-55.1	630.4	176.6
	25 group	389.8	-117.2	395.2	46.2

The same trend can be observed in the data from the super cell calculation, but with slightly higher magnitudes in the error. The results indicate that the cross sections prepared with the super cell are very consistent with those prepared with the full core approach.

Table 3: Differences in k-effective (pcm) between Xuthos and Serpent with SC cross section set

		Case 1	Case 2	Case 3	Case 4
Xuthos	2 group	1569.5	541.1	2102.4	1096.4
	9 group	588.5	-28.9	679.9	212.8
	25 group	413.8	-126.5	406.1	37.2

The next step in the analysis of the results is to examine the differences in the power distributions obtained between Serpent and Xuthos. The seven fuel blocks in the model are labeled in Fig 6. It is important to recall that regions 2-6 use the same cross section set, which will explain some of the differences in the results.

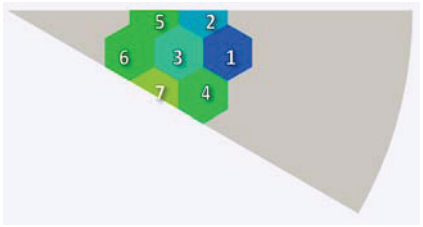

Fig. 6: Assembly map for power reporting.

The percent errors in the normalized block powers for the four cases are shown in Table 4. In a similar way as with the eigenvalue results, the prediction of the block powers consistently improve with increasing number of groups in the core calculation. Blocks 5 and 6 have the highest errors in all of the calculations. These blocks are located near the inner reflector, where the spectrum quickly changes when neutrons from the reflector penetrate the core. The errors originate from the improper cross section homogenization of the burned fuel region and we can conclude that more spectral zones are required to reduce the error. The best estimate of the block 1 power occurs in case 2.

In all cases the errors of the BP blocks with 9 groups are within 4%. These are reduced below 3% with the 25 groups structure. For case 1 and case 3,

the 25-group structure does not reduce the error significantly, just over 1%. The 2-group results are generally not acceptable because the error is significantly larger around 10%.

With 9 groups, the difference between SC and FC results for all cases are smaller than 0.5%. With 25 groups, the differences are even smaller around 0.1%. Therefore, we note that the cross sections produced with the super cell can represent those from the full core model with great accuracy when the number of energy groups is greater than or equal to 9.

Table 4: Percent Error of normalized block powers of Xuthos versus the Monte Carlo reference

(a) Case 1

ID	Serpent power	2Group		9Group		25Group	
		FC [a]	SC [b]	FC	SC	FC	SC
1	4.179E-1	8.0[c]	9.4	3.4	3.8	2.5	2.6
2	6.939E-2	3.2	2.7	1.8	1.6	1.7	1.7
3	1.161E-1	1.7	2.7	1.0	1.2	0.6	0.7
4	1.405E-1	1.2	1.9	1.0	0.8	1.3	1.2
5	6.418E-2	11.3	12.5	6.0	6.3	5.0	5.1
6	1.361E-1	**16.2**	**17.5**	**8.1**	**8.4**	**6.7**	**6.8**
7	5.580E-2	4.9	6.1	1.6	1.9	1.0	1.1

a - with FC cross section set
b - with SC cross section set
c- error in percent

(b) Case 2

ID	Serpent power	2Group		9Group		25Group	
		FC	SC	FC	SC	FC	SC
1	3.369E-1	7.0	8.5	1.1	1.4	0.3	0.3
2	6.492E-2	3.9	3.6	1.7	1.6	1.6	1.6
3	1.283E-1	0.6	0.2	0.7	0.6	0.9	0.9
4	1.376E-1	0.6	0.1	1.4	1.3	1.6	1.6
5	8.113E-2	7.4	8.3	2.4	2.6	1.8	1.8
6	1.843E-1	**11.4**	**12.4**	**3.5**	**3.7**	**2.6**	**2.6**
7	6.681E-2	1.2	2.1	1.0	0.9	1.3	1.3

(c) Case 3

ID	Serpent power	2Group		9Group		25Group	
		FC	SC	FC	SC	FC	SC
1	4.762E-1	9.9	10.9	3.9	4.2	2.7	2.8
2	5.874E-2	4.3	3.6	1.8	1.6	1.6	1.6
3	1.027E-1	4.5	5.5	2.1	2.3	1.3	1.4
4	1.269E-1	2.9	3.7	0.5	0.3	1.0	1.0
5	5.896E-2	16.1	17.2	7.6	7.9	5.9	6.0
6	1.251E-1	**21.4**	**22.6**	**9.8**	**10.1**	**7.7**	**7.8**
7	5.146E-2	9.6	10.6	2.9	3.2	1.6	1.7

(d) Case 4

ID	Serpent power	2Group		9Group		25Group	
		FC	SC	FC	SC	FC	SC
1	4.077E-1	10.1	11.4	3.1	3.4	1.9	1.9
2	5.749E-2	5.2	4.6	1.9	1.8	1.7	1.6
3	1.137E-1	2.3	3.2	0.7	0.9	0.2	0.2
4	1.279E-1	1.0	1.6	1.0	0.8	1.4	1.3
5	7.188E-2	12.5	13.6	4.8	5.0	3.6	3.6
6	1.611E-1	**17.0**	**18.2**	**6.3**	**6.5**	**4.8**	**4.7**
7	6.025E-2	6.1	7.1	1.0	1.2	0.1	0.1

V.B. Results of other deterministic neutronic packages

Only case 1 with the FC cross section set is selected for the INSTANT calculations. Similar behavior has been obtained for other cases. Results are showed in Table 5.

Table 5: INSTANT results of case 1 with 2 groups

p_{surf}		1	2	3	4
PN order	1	1.086739[a]	1.087231	1.087246	1.087251
		122.7[b]	171.9	173.4	173.9
		0.359[c]	0.570	0.577	0.579
	3	1.084656	1.085563	1.085593	1.085600
		-85.6	5.1	8.1	8.8
		0.364	0.0176	0.0288	0.0317
	5	1.084517	**1.085500**	1.085531	1.085538
		-99.5	**-1.2**	1.9	2.6
		0.416	**0.00516**	0.00632	0.00934
	7	1.084481	1.085487	1.085518	1.085525
		-103.1	-2.5	0.6	1.3
		0.429	0.00965	0.00180	0.00458
	9	1.084470	1.085483	1.085513	1.085520
		-104.2	-2.9	0.1	0.8
		0.433	0.0112	0.000472	0.00296

a - k-effective
b - error of k-effective in pcm
c - maximum error of normalized assembly powers in percent

The errors of the P_1 results are significantly larger than the ones from the higher PN orders. Errors of the results with p_{surf} equal to 1 are also significantly larger due to the interfering between angular discretization and spatial discretization. We notice that with unstructured triangular mesh, the minimum p_{surf} should be 2. We see a much faster convergence with respect to p_{surf} than with respect to PN order. The increasing errors of block powers with respect to the p_{surf} are due to the cancellation of errors caused by the finite PN orders. With PN=9 and p_{surf}=4 and with the initial grid, we can make the error of k-effective within 1 pcm. However, comparing with the error introduced by homogenization and condensation, the discretization error is quite small, so P_5 and the quadratic shape function can give us good results.

Calculations are also performed with 25 groups. Results are shown in Table 6 where it is evident that the cancellation error is not as significant as in the 2-group results. Again, P_5 and the quadratic shape function can give us good results.

Table 6: INSTANT results of case 1 with 25 groups.

p_{surf}		1	2	3
PN order	1	1.07703245 90.415 0.293	1.0770745 94.617 0.380	1.0770731 94.476 0.382
	3	1.07599 -13.83 0.189	1.0761131 -1.517 0.00107	1.0761136 -1.469 0.00151
	5	1.07599061 -13.769 0.210	**1.0761194** **-0.889** **0.00619**	1.0761205 -0.784 0.00377
	7	1.07599254 -13.576 0.215	1.0761235 -0.476 0.00538	- - -
	9	1.0759932 -13.51 0.216	1.0761249 -0.341 0.00533	- - -

The errors in the block powers for case 4 using the SC cross sections in Pronghorn and INSTANT compared to the deterministic reference from Xuthos are presented in Table 7. We note that algebraic 2(p+1) convergence on k-effective with uniform mesh refinement is observed in Pronghorn. Pronghorn results are generated with linear shape functions on a 4 time uniformly refined mesh. For case 4 this mesh had the error in k-effective of less than 1pcm. INSTANT results are generated with P_5 and p_{surf}=2. We see that PN results with INSTANT match the Xuthos results very well. Errors in the diffusion calculations are within 2%. However, comparing with the reference MC results, Pronghorn results are slightly better than the Xuthos results, as showed in Table 8, due to the cancellation of the dominant errors associated with the multigroup cross sections.

Table 7: Deterministic power results for case 4 .

2 Groups			
Block	% Difference from Reference		Reference Power of Xuthos
	Pronghorn	INSTANT	
1	0.161	0.0032	0.4541
2	1.148	0.0025	0.0601
3	0.383	0.0015	0.1100
4	0.228	0.0006	0.1258
5	0.606	0.0050	0.0621
6	1.259	0.0076	0.1318
7	0.173	0.0032	0.0560
9 Groups			
1	0.331	0.0051	0.4215
2	1.431	0.0027	0.0585
3	0.424	0.0023	0.1127
4	0.234	0.0012	0.1290
5	0.796	0.0068	0.0683
6	1.553	0.0100	0.1505
7	0.222	0.0042	0.0595
25 Groups			
1	0.379	0.0289	0.4155
2	1.567	0.0382	0.0584
3	0.482	0.0529	0.1135
4	0.215	0.0265	0.1296
5	0.859	0.0397	0.0693
6	1.686	0.0107	0.1534
7	0.222	0.0467	0.0602

Table 8: Power results for case 4 with 25 groups.

Case 4, 25 G	% Difference from Reference		Reference Power
Assembly	Pronghorn	Xuthos	Serpent
1	1.533	1.919	0.4077
2	0.057	1.650	0.0575
3	0.658	0.177	0.1137
4	1.119	1.337	0.1279
5	2.778	3.606	0.0719
6	3.141	4.746	0.1611
7	0.146	0.076	0.0602

A comparison of critical eigenvalue results is also presented in Tables 9 for each of the four cases with SC cross sections. Uniform mesh refinement is performed for the Pronghorn calculations with the linear shape functions. The results show errors less than 1 pcm caused by spatial discretization. RattleSnake results are generated with 4 polar angles and 6 azimuthal angles and with quadratic shape functions in space. RattleSnake produces consistent results.

Table 9: Eigenvalue results

(a) case 1 with Serpent reference 1.07223.

Groups	2	9	25
Pronghorn	-1648	-592	-375
RattleSnake	-1574	-590	-417
INSTANT	-1568	-588	-413
XUTHOS	-1570	-589	-413

(b) case 2 with Serpent reference 1.00020.

Groups	2	9	25
Pronghorn	-674	-87	35
RattleSnake	-543	24	124
INSTANT	-541	28	126
XUTHOS	-541	29	127

(c) case 3 with Serpent reference 1.07504.

Groups	2	9	25
Pronghorn	-2174	-697	-395
RattleSnake	-2109	-682	-413
INSTANT	-2101	-678	-404
XUTHOS	-2102	-680	-406

(d) case 4 with Serpent reference 1.01650.

Groups	2	9	25
Pronghorn	-1177	-262	-66
RattleSnake	-1096	-201	-22
INSTANT	-1098	-215	-39
XUTHOS	-1096	-213	-37

IV. CONCLUSIONS

The results show that the Serpent generated cross sections do not accurately reproduce the reference Monte Carlo solution in all cases. The BP treatment (Case 4) produces good results, but this is mainly due to error cancellation.

With regard to the energy group structure, the 2-group calculations produce results that are generally not acceptable without the use of equivalence theory parameters. The 9-group can be used for scoping calculations and the 25-group structure delivers consistently improved results.

One clear outcome is that the super cell approach yields cross sections that are consistent with those prepared with an "exact" full core calculation; as long as the number of coarse groups is 9 or higher.

With the BP treatment and homogenization, PN order 5 or 4 polar angles and 6 azimuthal angles are sufficient for the angular discretization. Spatial polynomial order 2 is recommended. In addition, very good agreement exists between the various deterministic transport and diffusion codes in both eigenvalue and power distributions.

Future research will focus on improving the cross sections and better understanding the cancellation of errors that take place. Furthermore, detailed pin structure calculations are necessary to conclude this research successfully.

V. ACKNOWLEDGEMENTS

This work is supported by the U.S. Department of Energy, Assistant Secretary for the office of Nuclear Energy, under DOE Idaho Operations Office Contract DEA07-05ID14517

REFERENCES

[1] J. Ortensi: Proceedings of HTR 2012, 6th International Topical Meeting on High temperature Reactor Technology (HTR), Tokyo, Japan, October 28- November 24, 2012, HTR2012-5-023.

[2] IAEA-TECDOC-1382: Evaluation of high temperature gas cooled reactor performance: benchmark analysis related to initial testing of the HTTR and HTR-10, November 2003.

[3] H. Park, D. A. Knoll, D. R. Gaston, R. C. Martineau, Tightly Coupled Multiphysics Algorithms for Pebble Bed Reactors. Nucl. Sci. Eng., Vol. 166, p. 118–133, 2010.

[4] D. Gaston, C. Newman, G. Hansen, and D. Lebrun-Grandie, MOOSE: A Parallel Computational Framework for Coupled Systems of Nonlinear Equations, Nuclear Engineering and Design, Vol. 239(10), p. 1768-1778, 2009.

[5] J. Leppänen: Development of a New Monte Carlo Reactor Physics Code, D.Sc. Thesis, Helsinki University of Technology, VTT Publications 640, 2007.

[6] J. Leppänen: Randomly Dispersed Particle Fuel Model in the PSG Monte Carlo Neutron Transport Code, In *Proc. M&C + SNA 2007, Monterey, California, April 15–19, 2007*.

[7] Yaqi Wang, Cristian Rabiti, Giuseppe Palmiotti, Krylov Solvers Preconditioned with the Low-Order Red-Black Algorithm for The Pn Hybrid FEM for The INSTANT Code, Proc. International Conference on Mathematics and Computational Methods Applied to Nuclear Science and Engineering, Rio de Janeiro, Brazil, 2011.

[8] Yaqi Wang, Jean C. Ragusa, Mark DeHart, Xuthos: A Discontinuous Galerkin Transport Solver for NEWT Based on Unstructured Triangular Meshes, International Conference on Reactor Physics, Nuclear Power: A Sustainable Resource, Casino-Kursaal Conference Center, Interlaken, Switzerland, September 14-19, 2008.

[9] Frederick N. Gleicher II, Yaqi Wang, Derek Gaston, Richard C. Martineau, The Method of Manufactured Solutions for RattleSnake, A SN Radiation Transport Solver inside the MOOSE Framework, ANS summer meeting, 2012.

[10] B. S. Kirk, J. W. Peterson, R. H. Stogner, and G. F. Carey. `libMesh`: A C++ Library for Parallel Adaptive Mesh Refinement/Coarsening Simulations. *Engineering with Computers*, 22(3-4):237-254, 2006.

[11] Larry A. Schoof, Victor R. Yarberry, EXODUS II: A Finite Element Data Model, SAND92-2137, 1995.

[12] M.A. Pope, J. Ortensi, A.M. Ougouag: Investigation of Supercells for Preparation of Homogenized Cross Sections for Prismatic Deep Burn VHTR Calculations, *5th International Conference on High Temperature Reactor Technology*, HTR 2010, October 2010.

[13] V. Descotes, M.A Pope, J. Ortensi, A. Hebert, "Studies of 2-D Reflector Effects in Cross Section Preparation for Deep Burn VHTRs," *Nuc. Eng. Des.* 242, pp. 148-156, January 2012.

[14] "OECD/NEA/NSC PBMR Coupled Neutronic/Thermal Hydraulics Transient Benchmark: The PBMR-400 Core Design," Draft 07 (2007).

[15] Yaqi Wang, Jean C. Ragusa, Standard and Goal-Oriented Adaptive Mesh Refinement Applied to Radiation Transport on 2D Unstructured

Triangular Meshes, Journal of Computational Physics, Vol. 230:3, p763-788, 2011.

[16] I. Dilber and E. E. Lewis, Variational Nodal Methods for Neutron Transport. Nucl. Sci. Eng., Vol. 91, p. 132, 1985.

[17] J. E. Morel and J. M. McGhee. A Self-Adjoint Angular Flux Equation. Nucl. Sci. Eng., Vol. 132, p. 312–325, 1999.